JMEPEG (2008) 17:550–560
DOI: 10.1007/s11665-007-9165-5

1059-9495/$19.00

Wear Evolution in a Stranded Rope Subjected to Cyclic Bending

Mikel Aingeru Urchegui, Wilson Tato, and Xabier Gómez

(Submitted May 7, 2007; in revised form June 18, 2007)

Wire ropes, due to their construction, combine two very interesting properties: high axial strength and flexibility in bending. However, the assemblage of wires to form flexible ropes results in the sliding of contacting wires and the creation of wear scars, which can act as stress risers and reduce the fatigue life of ropes. Therefore, in order to understand the fatigue behavior of wire ropes, the degradation that occurs between the wires and the strands has to be studied first. In this study, after identifying the main wear patterns for a polymer-covered stranded rope, the wear evolution along the number of cycles and the effect of the sheave diameter in the preferential wear sites were analyzed. The tests were carried out in a custom-made Bending over Sheave (BoS) fatigue test bench and short segments of the rope were analyzed by Scanning Electron Microscope (SEM) and confocal imaging profilometry in order to characterize the wear scars. The worn volume and the wear scar depth were selected as the most suitable parameters to characterize the wear behavior of wires. In addition, the importance of the polymeric cover and sheave diameter was proved: a reduction of the sheave diameter results in a bigger wear rate (μm^3/cycle).

Keywords Bending over Sheave (BoS) tests, steel wires, wear, wire rope

1. Introduction

Steel wire ropes are composed of individual steel wires wound into bundles called strands, which are then wound into the final rope. A wire rope is identified by its construction: the way its wires have been laid to form the strands and the way its strands have been laid around the core (Right Regular, Left Regular, Right Lang, Left Lang, and Right Alternate), number of strands and geometric arrangement of the wires in the strands (Warrington, Seale, Filler Wire, etc.). A complete description of wire ropes identification and construction can be found in a publication produced by the American Iron and Steel Institute (AISI) (Ref 1).

Due to their construction, wire ropes combine two very interesting properties: high axial strength and flexibility in bending. These properties convert wire ropes into very useful elements for many industrial applications, e.g., mine hoisting, lifts, bridges, barges, tyres, etc. The assemblage of wires to form flexible ropes results in the sliding of individual wires against their neighboring wires whenever the rope passes over a sheave or is put under tension. These movements between contacting wires cause the wear of wires by fretting or reciprocating sliding, and reduce the fatigue life of ropes (Ref 2-8).

Mikel Aingeru Urchegui, Wilson Tato, and **Xabier Gómez**, Mondragon Goi Eskola Politeknikoa, Mondragon Unibertsitatea, Loramendi 4, 20500 Arrasate-Mondragon, Spain. Contact e-mail: murchegui@eps.mondragon.edu.

Whatever the application is, the wire rope will suffer fatigue. Depending on the application, wire ropes may be subject basically to two types of fatigue: Tension-Tension (T-T) fatigue, where a fluctuating tensile load is superimposed to a mean tensile load (i.e., bridges), and Bending over Sheave (BoS) fatigue, where a constant tensile load is combined with repeated bending (as the rope runs on and off a sheave). However, the great majority of applications (cranes, lifts, etc.) will subject the rope to bending fatigue.

Over the last years, several improvements have been made in the understanding of the behavior of steel wire ropes. Some works examined the way in which the bending fatigue performance of ropes changed with working conditions: Chaplin and Potts (Ref 9) studied the effect of some parameters (load level, ratio between sheave diameter and rope diameter, length of rope subjected to bending, wrapping angle, sheave groove geometry, etc.) on the fatigue life of ropes; Ridge et al. measured the cyclic bending strains in the wires of a steel wire rope running on and off a pulley (Ref 10), and investigated the effects of simulated degradations (wire breaks, plastic deformation, abrasive wear, corrosion, slack strands, slack wires, etc.) on the rope's BoS fatigue endurance (Ref 11); Feyrer's studies (Ref 12-16) were focused on developing methods of calculating the life of wire ropes subject to BoS fatigue; and other studies analyzed the failure of ropes in real applications (Ref 17-20). In summary, the aim of these studies was to determine the fatigue endurance of ropes under different conditions but without analyzing the effect of the working conditions on the wear rate.

In order to acquire a better understanding of the fatigue behavior of ropes, the degradations that occur between contacting wires should also be studied: the wear of wires reduces the cross section of the rope and its load carrying capability. Furthermore, the wear scars can act as stress risers decreasing the fatigue life of the rope. These wear scars are the result of one of three different contact types (Ref 21):

(a) contact of the outer strands of the rope with an external element, such as a sheave (commonly called crown wear); (b) line contacts between wires within a single strand; and (c) point contacts between wires within a single strand or between strands. Interstrand point contacts are collectively known as trellis contact or nick.

Therefore, the objective of this study is to determine the wear evolution along the number of cycles and analyze the effect of the sheave diameter on the wear rate of a stranded rope employed in hoisting devices. The rope was tested under different working conditions in a custom-made BoS fatigue test bench, and short segments of the rope were examined in order to determine the size, depth and worn volume of the wear scars caused by the different interwire contact types. In this study, the definition and designation of the different contact types is based on the definitions and designations provided by Schrems et al. (Ref 21).

2. Experimental Details

2.1 Tested Rope

The rope used in this study was a stranded steel wire rope (7×19) covered with a polymeric sheath (Fig. 1a), with a minimum breaking load of 22.5 kN. The nominal diameter of the rope (including the cover) was 6.5 mm and the nominal diameter of the metallic part was 5.0 mm. The core was a Warrington right lay strand and the outer layer consisted of 6 Seale strands wound around the core in a right regular lay direction (Fig. 1b). All wires were flash brass-plated and their diameters ranged from 0.22 to 0.45 mm. The wires material was a cold-drawn eutectoid carbon steel (0.8% C) with a Tensile Strength over 2800 MPa and a hardness of 659 ± 81 HV0.05.

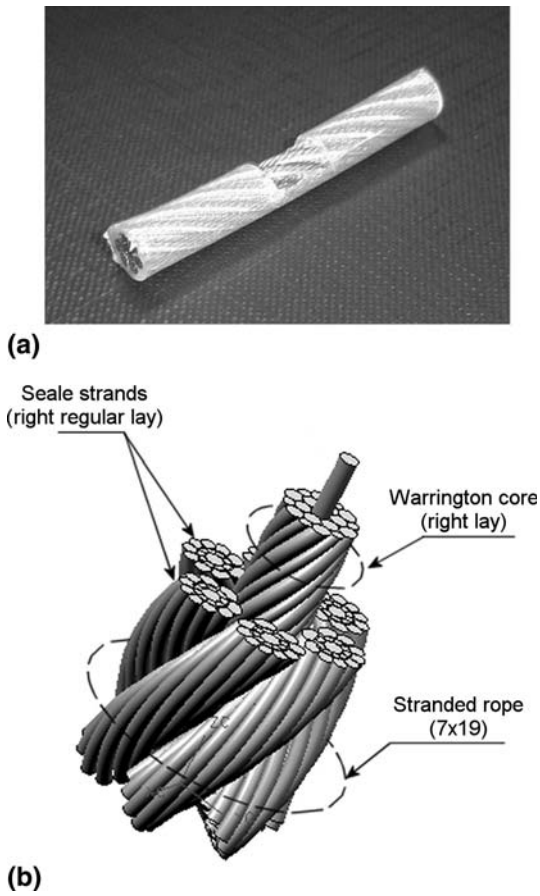

Fig. 1 Details of the wire rope: (a) rope with polymeric cover and (b) construction of the metallic part

With the construction of this rope, three different wear patterns were identified (Fig. 2): (a) linear wear scars, due to the contacts of the central wire of strands with the wires of the inner layer and the contacts of adjacent wires within the same layer; (b) wear scars caused by interstrand point contacts due to the interaction of the wires of the outer layer of strands with the wires of the outer layer of the core, called in this study "nick type A"; and (c) wear scars caused by interstrand point contacts due to the interaction of the wires of the outer layer of adjacent strands, called in this study "nick type B."

Schrems et al. (Ref 21) defined another wear pattern due to the contact of the strands with an external element (sheave) but, in this rope, the polymeric cover avoids such a contact.

Although linear wear scars were identified in all wires, all of them could be classified in six big groups: linear wear scars due to the contacts between the central wire of the core and the wires of the inner layer of the core; linear wear scars due to the contacts between adjacent wires of the inner layer of the core; linear wear scars due to the contacts between adjacent wires of the outer layer of the core; linear wear scars due to the contacts between the central wire of strands and the wires of the inner layer of strands; linear wear scars due to the contacts between adjacent wires of the inner layer of strands; and linear wear scars due to the contacts between adjacent wires of the outer layer of strands. Each of these groups will present its own wear evolution but, in this article, the wear behavior of one of these groups was analyzed: linear wear scars due to the contacts between the central wire of the core and the wires of the inner layer of the core.

Nicks type A can be found in the outer wires of the core or in the outer wires of the strands. Moreover, three different characteristic nicks can be identified at the strands-core contacts: one on the large wires of the outer layer of the core, one on the small wires of the outer layer of the core, and another on the wires of the outer layer of strands. The nicks on the outer wires of the strands can be caused by the contact with the large wires of the outer layer of the core or by the small ones. Therefore, when a wire of the outer layer of the strands is analyzed, it is not known if the wear scar is caused by the large or the small wire of the outer layer of the core. On the other hand, the wear scars on the small wires of the outer layer of the core, although their sizes will be different to the wear scars found in the large wires, their evolution could be similar to the evolution of the wear scars on the large wire. This fact will be analyzed in a next study. Consequently, the large wires of the outer layer of the core were selected to analyze the nick type A evolution.

Finally, nicks type B can only be found in the outer wires of the strands so these wires were chosen to analyze its evolution.

In Fig. 3, SEM micrographs of the identified wear patterns are shown. The shape differences between nick type A and nick type B are due to the different crossing angle between the contacting wires, 5° and 45°, respectively: as the crossing angle decreases, a more elliptical wear trace is created.

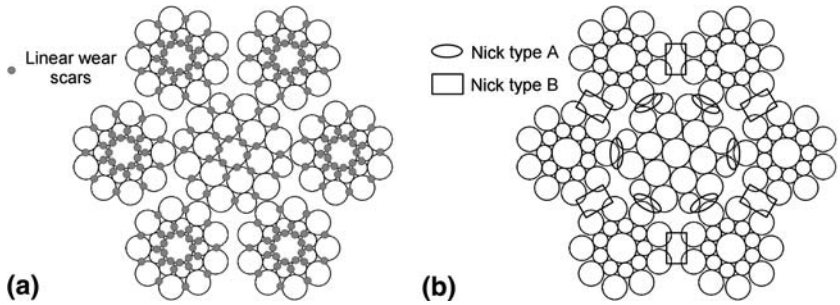

Fig. 2 Cross section of the rope with the location of the different wear patterns: (a) location of linear wear scars; and (b) location of nicks type A and nicks type B

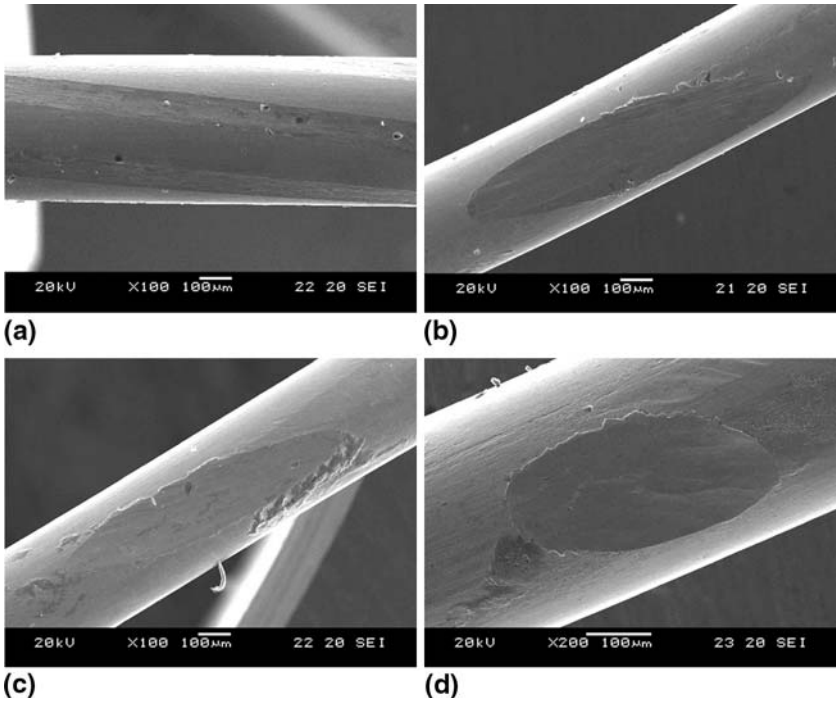

Fig. 3 SEM micrographs of wear scars: (a) linear wear scar; (b) nick type A on the large wire of the outer layer of the core; (c) nick type A on a wire of the outer layer of strands, and (d) nick type B

2.2 Test Facilities

The test machine was an accelerated BoS fatigue test bench specially designed for this study, with a reciprocating forth and back motion. The test bench is 20 m height. In Fig. 4, a drawing of the test machine is shown. The traction system employed was mounted on the upper part of the test bench and consisted in a gearless electric machine (slow speed motor) connected to a 200 mm in diameter traction sheave. At the bottom part of the test machine, a 200 mm in diameter tension sheave was mounted, in which a tensile load of 3 kN was applied. Two reflective optical sensors were placed in the test machine structure to control the forth and back motion of the traction sheave, applying a certain vertical separation between them (6 m) to adjust the rope stroke. A plastic cylinder covered with reflective material had to be mounted on the rope in order to assure the detection of the rope position with the optical sensors.

Between the traction sheave and the tension sheave, a set of four identical polyamide deflection sheaves was mounted, with a vertical separation of 1.50 m between them. The purpose of this set is to obtain four specimens with different number of cycles in a single test. Adjusting the rope stroke correctly, four different rope segments can be identified (Fig. 5): when the traction sheave completes the forth motion, the segment 4 has passed over the four deflection sheaves, the segment 3 over three deflection sheaves, the segment 2 over two deflection sheaves, and segment 1 over a single deflection sheave. The same sequence is repeated when the traction sheave completes the back motion. Therefore, when the traction sheave completes one reciprocating cycle, segments with two, four, six, and eight BoS cycles are obtained. Neither the traction sheave nor the tension sheave is reached by the four analyzed specimens.

2.3 Test Program and Analysis Procedure

The objective of this study is to analyze the wear evolution along the number of cycles and to determine the influence of the sheave diameter in the preferential wear sites of a stranded rope employed in hoisting devices. Hence, the remaining parameters were kept constant: the tensile load applied to the rope was 3 kN, the rope velocity 3.2 m/s, and the wrap angle in every sheave was 180°.

The deflection sheaves were manufactured in polyamide with a circular groove. The standards (Ref 22) establish a minimum ratio D/d of 40 (ratio between sheave diameter D, and rope diameter d). Nowadays however, one of the main objectives in hoisting applications is to reduce the size and weight of equipments, and the installation space saved for the hoisting device. One way to achieve this objective is to reduce the sheaves diameters. So, if this strategy is selected, the guidelines provided by the standard cannot be fulfilled and the consequences of reducing the D/d ratio should be studied. Therefore, three different sets of sheaves were employed in this study: the first with 200 mm diameter sheaves (ratio $D/d = 40$), the second with 150 mm diameter sheaves (ratio $D/d = 30$), and the third with 100 mm diameter sheaves (ratio $D/d = 20$).

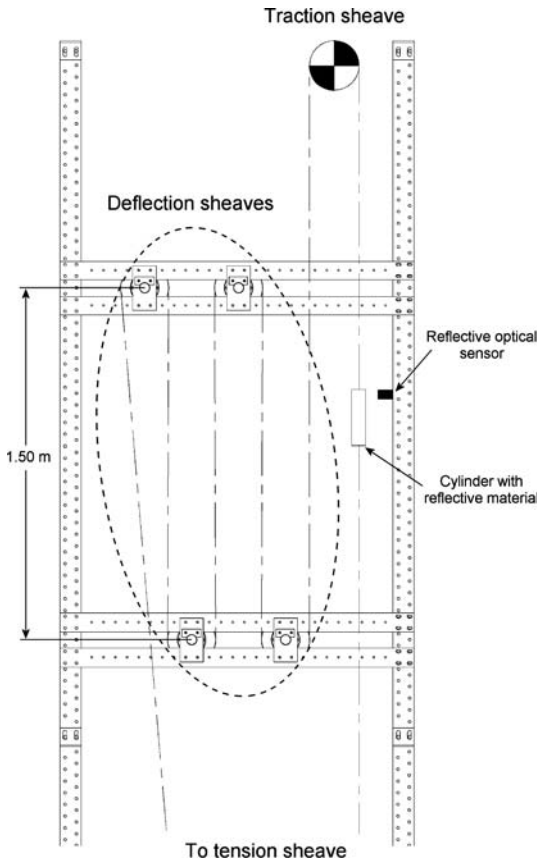

Fig. 4 Drawing of test machine

With an applied tensile load of 3 kN, the safety factor is 7.5. Although it seems that this safety factor is generous, the standards (Ref 22) establish that the safety factor for the selected rope ($d = 5$ mm), running over a 200 mm diameter sheave (ratio $D/d = 40$), the minimum safety factor should be 12. Moreover, with smaller deflection sheaves, this safety factor should be greater. Therefore, wear in typical application would be expected to be smaller than the wear obtained for the tests carried out in this study.

The test program was developed varying the number of cycles and the deflection sheaves diameters (Table 1). The maximum number of cycles for each sheave diameter was obtained checking the rope integrity along the BoS cycles and stopping the test before the rope failure: 1600×10^3 cycles, 800×10^3 cycles, and 80×10^3 cycles for tests carried out over 200, 150, and 100 mm deflection sheaves, respectively. A cycle was defined as the straight-bent-straight sequence of the rope. A new rope was also analyzed in order to know the initial condition of the wires.

The analysis procedure consists basically in two steps: (a) wear scars measurement and worn surfaces analysis using SEM; and (b) three-dimensional topographies acquisitions by means of confocal imaging profilometry.

The wear scars sizes were obtained as the main value of the measurement of three different scars. Due to the characteristics of the linear wear scars, the width was measured. To obtain the width, the wires were placed in such a way that the wear scars were in horizontal direction (Fig. 6a). Nicks type A and nicks type B present a hyperbolic paraboloid shape, with the ratio of the major axis to minor axis (elliptical trace in two dimensions) a function of the helix angles of the two wires in contact: the larger difference in helix angle, the smaller ratio, and vice versa. Therefore, wires where nicks type A or nicks type B appeared were placed in such a way that the major axis of the elliptic wear scar was in horizontal direction, and the major (M) and minor (m) axes of these wear scars were measured (Figs. 6b and c).

To obtain the wear scars depth and worn volumes, three-dimensional topographies were acquired by confocal imaging profilometry. This technique provides reproducible resolution in height better than 5 nm whereas the best lateral resolution is

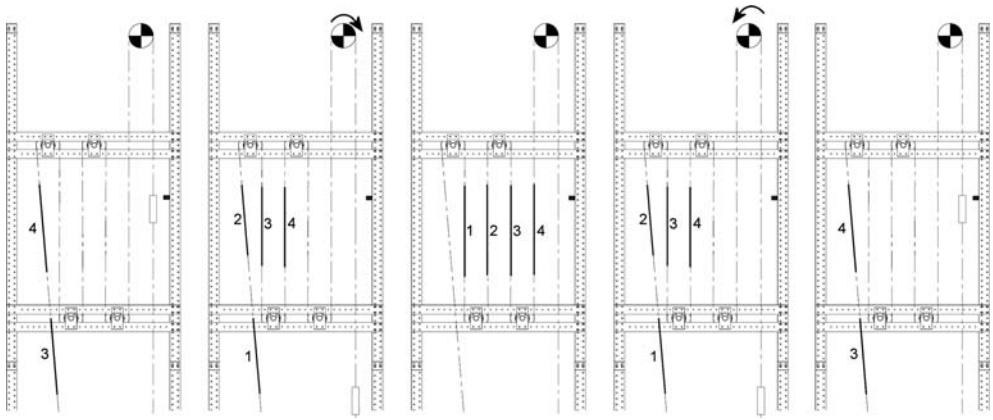

Fig. 5 Schematic sequence of the forth and back motion in the test machine

Table 1 Test program and analyzed specimens

Test conditions					Analyzed specimens	
Test ID.	Tensile load, N	Rope velocity, m/s	Sheaves diameter, mm	Cycles in traction sheave, 10^3	Specimen ID.	BoS cycles, 10^3
T00	...	...	...	0	T00-S01	0
T01	3000	3.2	150	100	T01-S01	200
					T01-S02	400
					T01-S03	600
					T01-S04	800
T02	3000	3.2	150	20	T02-S01	40
					T02-S02	80
					T02-S03	120
					T02-S04	160
T03	3000	3.2	200	200	T03-S01	400
					T03-S02	800
					T03-S03	1200
					T03-S04	1600
T04	3000	3.2	200	25	T04-S01	50
					T04-S02	100
					T04-S03	150
					T04-S04	200
T05	3000	3.2	100	10	T05-S01	20
					T05-S02	40
					T05-S03	60
					T05-S04	80
T06	3000	3.2	100	5	T06-S01	10
					T06-S02	20
					T06-S03	30
					T06-S04	40
T07	3000	3.2	100	1	T07-S01	2
					T07-S02	4
					T07-S03	6
					T07-S04	8

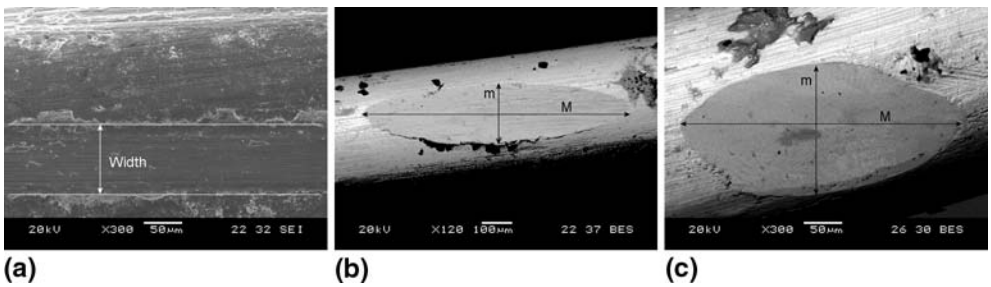

Fig. 6 Measured parameters in SEM: (a) linear wear scar; (b) nick type A; and (c) nick type B

0.18 μm (Ref 23). In linear wear scars, due to their characteristics, worn volume (volumetric wear) cannot be obtained so the planimetric wear and the wear scar depth were selected as representative parameters for this wear pattern (Fig. 7). The wear scar depth (h_{max}) was defined as the maximum distance between the worn profile and the profile of a new wire along its axis, and the planimetric wear (W_p) as the area enclosed between these profiles (calculated by numerical integration). To determine the volumetric wear (W_v) in nicks type A and nicks type B (Fig. 8), the surface of the unworn wire had to be estimated first. The volumetric wear was defined as the volume enclosed between the surface of the unworn wire and the surface acquired with the confocal imaging profiler whereas the wear scar depth was defined as the maximum vertical distance between both surfaces (h_{max}). The employed equipment, the acquisition methodology and the developed calculation algorithms were described in detail in a previous work (Ref 24).

3. Results and Discussion

3.1 Linear Wear Scars

The selected parameters for the characterization of linear wear scars are the wear scar width, depth, and planimetric wear. The wear scar width value was obtained for all specimens as the average value of three measurements carried out by SEM in three different scars of the same specimen. The standard deviation was less than 5% in all cases.

The first specimen analyzed was the central straight wire of the core of a new rope. This wire presented linear scars, due to the plastic deformations induced during the manufacturing process of the core. The width of this scar was 50 μm and will be considered as the starting point for this parameter. From this value, the evolution of this parameter along the number of cycles exhibits a similar behavior in tests accomplished over

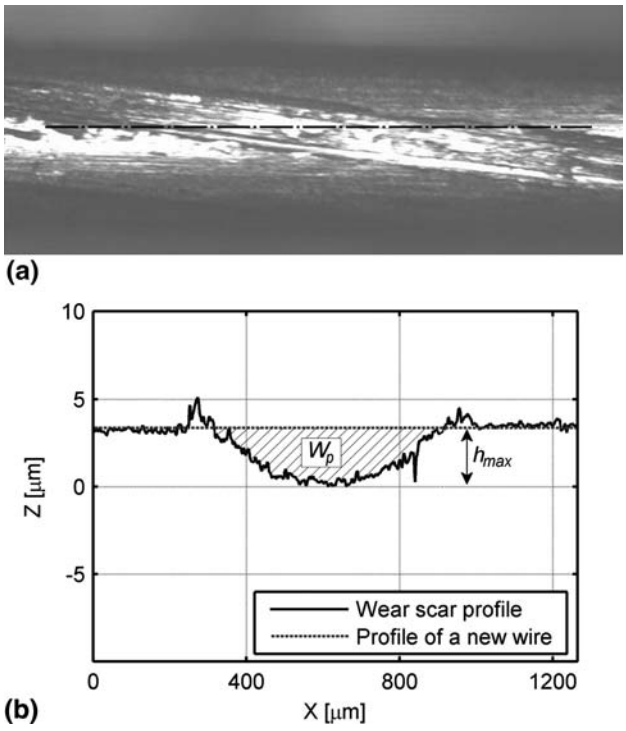

Fig. 7 Linear wear scar: (a) confocal image with 20× SLWD objective; (b) profile obtained along the dash-dot line and measured parameters

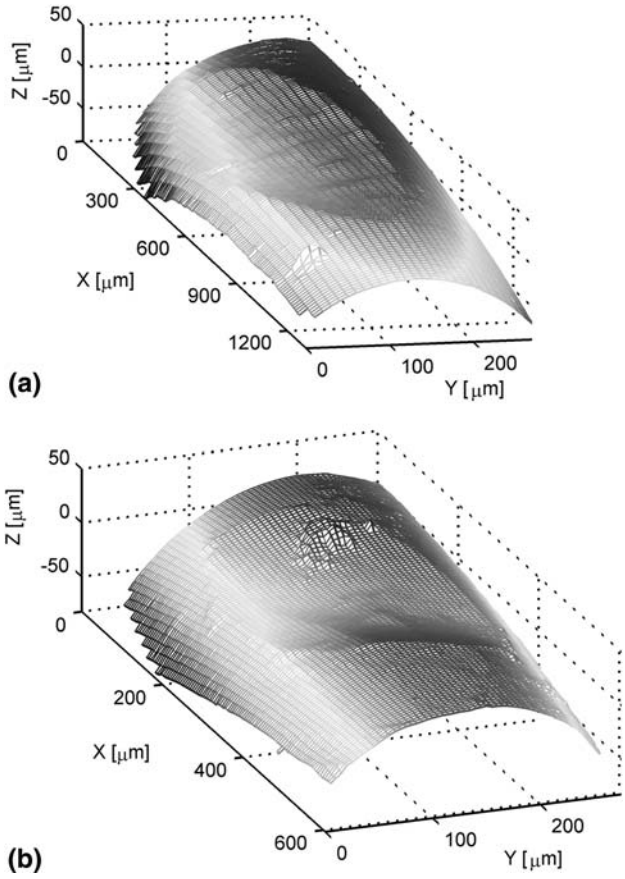

Fig. 8 Examples of three-dimensional topographies: (a) nick type A and (b) nick type B

different sheaves (Fig. 9): an initial short stage where the width value increases quickly up to 65-70 μm, and a constant slope stage where the wear scar width increases linearly for an increasing number of cycles. The transition between the two stages occurs at different number of cycles depending on the deflection sheaves diameters: 150×10^3 cycles, 80×10^3 cycles, and 10×10^3 cycles for tests carried out over 200, 150, and 100 mm deflection sheaves, respectively. Also the strong effect of sheaves diameter on the growing speed (slope of the linear stage) is clearly seen, especially when the smallest sheaves are employed: 0.64 μm/10^3 cycles for tests accomplished over 100 mm diameter sheaves, whereas the growing speed for tests carried out over 150 and 200 mm diameter sheaves is 0.063 μm/10^3 cycles and 0.024 μm/10^3 cycles, respectively.

Since the standard deviation of wear scars in wires belonging to the same specimens was rather small, to obtain the wear scar depth, and planimetric wear only a single three-dimensional topography was acquired for each specimen. In addition, the sensitivity of the topographic measurements was checked measuring the same scar three times: the standard deviation for the wear scar depth measurements was less than 4%, and less than 7% for planimetric wear results.

The evolution of these parameters along the number of cycles for each of the test sets is shown in Fig. 10. The first point in these graphics corresponds to the values obtained from the measurements performed in the wire of a new rope: a wear scar depth of 1 μm and a planimetric wear of 315 μm^2.

The wear scar depth evolution is similar to the behavior that exhibited the wear scar width, although the stage corresponding to a linear increase for an increasing number of cycles is not so clear. If the evolution of the planimetric wear is observed, an initial very short stage, where its value increases quickly up to 700 μm^2, can be seen for tests carried out over 200 and 150 mm diameter sheaves, followed by linear (constant slope) behavior. However, in tests accomplished over the smallest sheaves, this parameter exhibits rather linear behavior from the beginning. Also a strong effect of sheaves diameter on the wear rate can be derived: if the sheaves diameter is reduced from 200 up to 150 mm, the wear severity is multiplied by a factor of three, whereas a reduction of the sheaves diameter from 150 to 100 mm increases the wear severity in a factor of seven (Table 2). This effect of the sheaves diameter is clearly seen in Fig. 11, where the planimetric wear of all tests is represented in the same graphic. Due to the large range covered by the number of cycles, the abscise axis had to be represented in logarithm scale. It can be seen how the number of cycles required to obtain the same planimetric wear decreases as the sheaves' diameters are reduced.

3.2 Nick Type A

These wear scars present a hyperbolic paraboloid shape, with the ratio of the major axis to minor axis about 4.3. The selected parameters for the characterization of this wear pattern are major axis, minor axis, depth, and volumetric wear.

The major axis and minor axis values were obtained following the same procedure explained previously for the scar width in linear wear scars. The maximum standard deviation was 15%, bigger than the deviation presented in linear wear scars. The origin of this scattering could be the lack of control during the manufacturing process, causing small differences in the crossing angles of strands and core and, therefore, different contact pressure values and wear scar shapes.

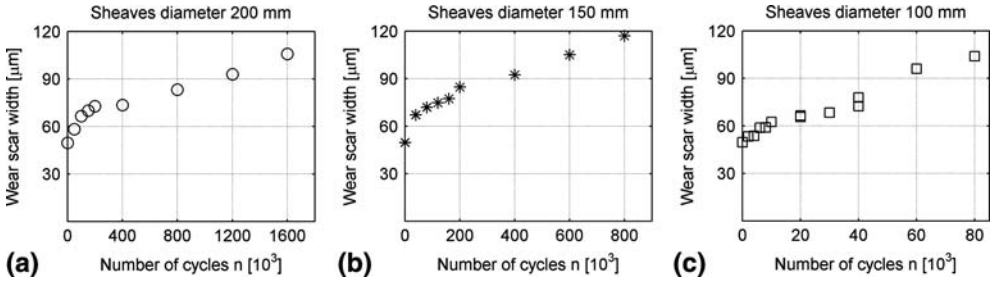

Fig. 9 Linear wear scars. Evolution of the wear scar width along the number of cycles: (a) sheaves diameter 200 mm; (b) sheaves diameter 150 mm; and (c) sheaves diameter 100 mm

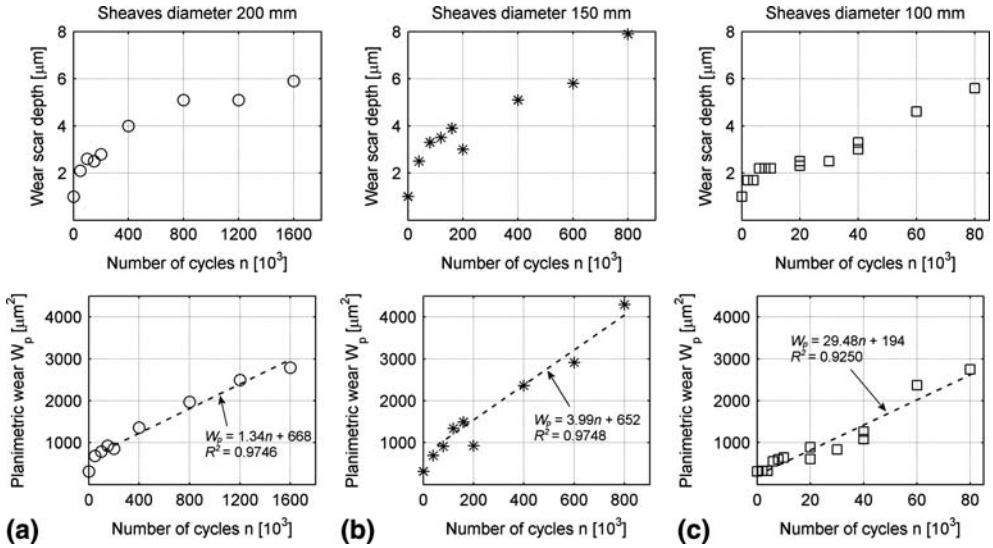

Fig. 10 Linear wear scars. Evolution of the wear scar depth and planimetric wear along the number of cycles: (a) sheaves diameter 200 mm; (b) sheaves diameter 150 mm; and (c) sheaves diameter 100 mm

Table 2 Linear wear scars: Results summary

		Sheaves diameter, mm		
		200	**150**	**100**
Linear wear scar	Maximum number of cycles, 10^3	1600	800	80
	Wear scar depth, μm	5.90	7.90	5.60
	Planimetric wear, μm^2	2792	4294	2749
	Wear rate, $\mu m^2/10^3$ cycles	1.34	3.99	29.48

The first specimens analyzed were the outer wires of the core of a new rope. Some small scars caused during the manufacturing process of the rope were identified. The average values for the major and minor axes measured were 640 and 81 μm, respectively. The evolution of both parameters along the number of cycles (Fig. 12) brings into view a first stage with decreasing slope, and a second stage with a smaller slope, approaching the major axis to 1200 μm and to 250 μm the minor axis. In Fig. 12c a decrease of the axes' values along the number of cycles can be seen from 40×10^3 cycles on. This tendency is physically impossible and is caused by the differences in crossing angles and limited number of measured wear scars. The standard deviation obtained for the axes (15%) has to be taken into account.

Before measuring the wear scar depth and volumetric wear of each specimen, the sensitivity of the topographic measurements was checked measuring a single wear scar three times: the standard deviation for the wear scar depth measurements was below 1%, and below 3% for volumetric wear results. Once the sensitivity of the topographic measurements was checked, three wear scars for each specimen obtained from tests carried out over 150 mm sheaves were analyzed in more detail in order to know the scattering in the wear scar depth and volumetric wear. The results of these measurements and the average value are shown in Fig. 13. Although some scars were identified by SEM for the wires belonging to a new rope, these scars could not be identified in the three-dimensional topographies. That is why the initial values for wear scar depth and volumetric wear are zero.

The maximum standard deviation for wear scar depth was 18% and 10% for volumetric wear. The reason for such important scattering in the wear scar depth could be the same

described for the axes scattering: the differences in contact pressure values and wear scar shapes derived from the manufacturing process. However, the scattering in the volumetric wear is smaller (10%). This fact could be attributed to the small effect of the pressure differences on the volumetric wear: some recent studies confirmed a linear evolution of the volumetric wear with the total accumulated dissipated friction energy (Ref 25-27), being this energy a function of the sliding amplitude and tangential (friction) force, but not a function of the contact pressure.

After having checked the scattering, the wear scar depth and planimetric wear of the remaining specimens were obtained from the topography of a single wear scar for each specimen. The evolution of the wear scar depth and volumetric wear along the number of cycles for each of the test set is shown in Fig. 14. The wear scar depth evolution presents a decreasing slope tendency, which could be approached by a square root function. The final depth is approximately 40 μm, and this value represents a local cross section reduction of 10% of the wire diameter. In addition to reduce the cross section, these wear scars become into stress risers making easier the fatigue failure. In Fig. 14c, a decrease of the wear scar depth values along the number of cycles can be seen again from 40×10^3 cycles on. The cause of this tendency is the same to this described for the axes. In this case, the standard deviation obtained for the wear

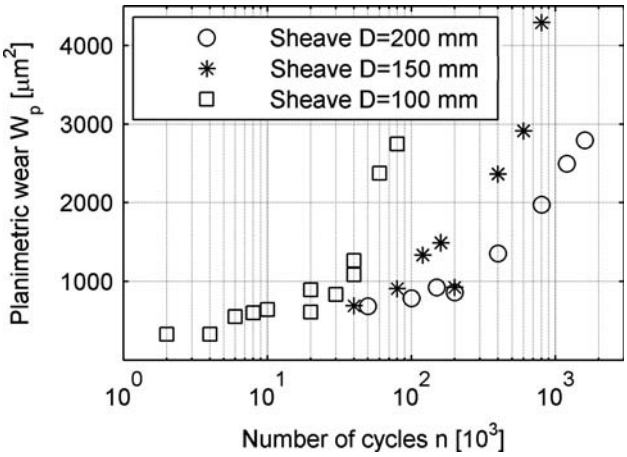

Fig. 11 Linear wear scars. Planimetric wear in all tests

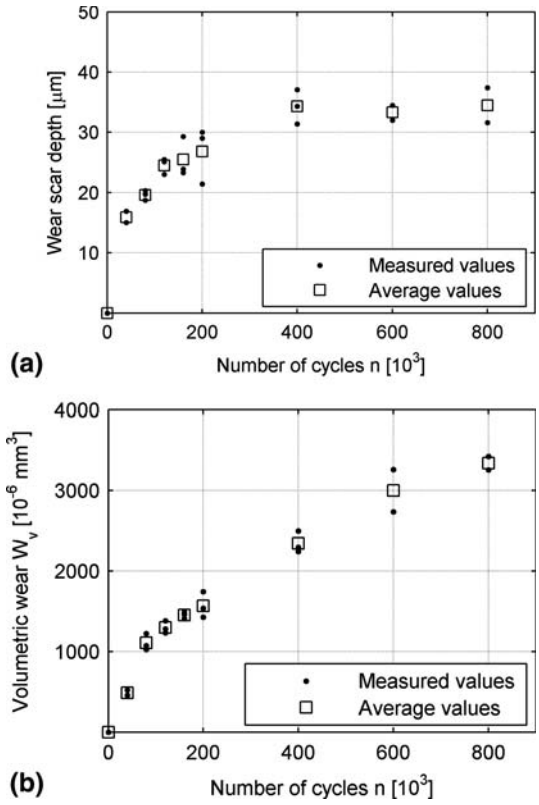

Fig. 13 Nick type A. Scattering and average values for wear scar depth (a) and volumetric wear (b) of specimens obtained form tests performed over 150 mm diameter sheaves

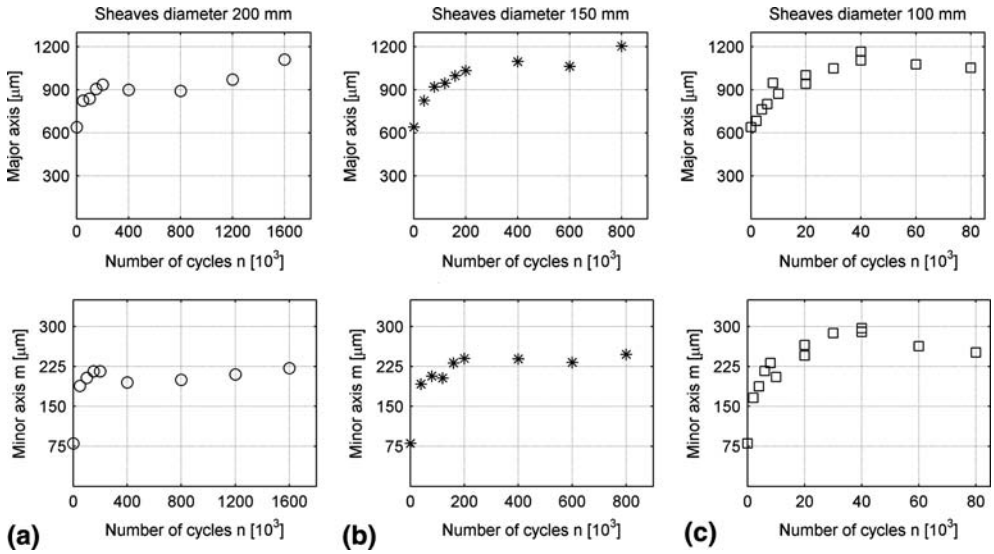

Fig. 12 Nick type A. Evolution of the major axis and the minor axis along the number of cycles: (a) sheaves diameter 200 mm; (b) sheaves diameter 150 mm; and (c) sheaves diameter 100 mm

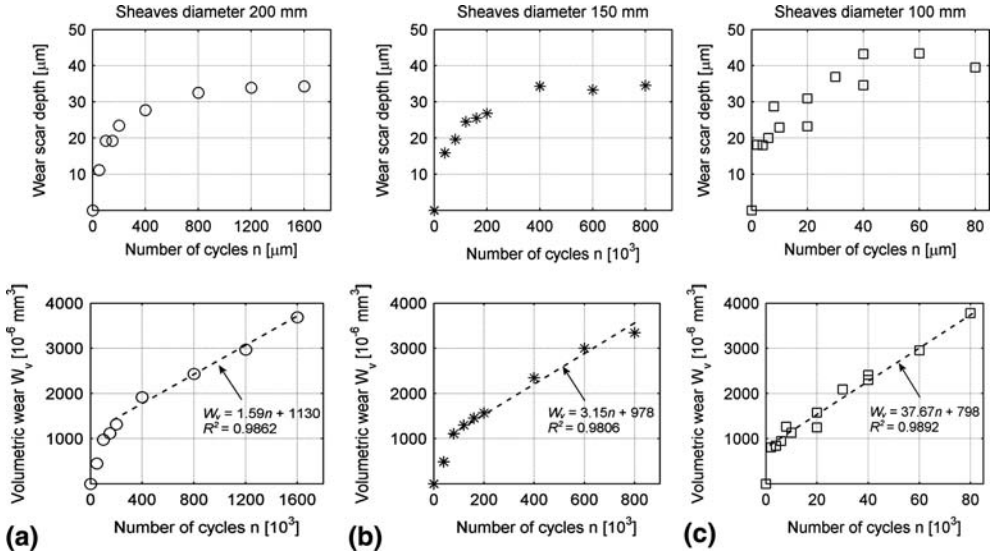

Fig. 14 Nick type A. Evolution of the wear scar depth and volumetric wear along the number of cycles: (a) sheaves diameter 200 mm; (b) sheaves diameter 150 mm; and (c) sheaves diameter 100 mm

Table 3 Nick type A: Results summary

		Sheaves diameter, mm		
		200	**150**	**100**
Nick type A	Maximum number of cycles, 10^3	1600	800	80
	Wear scar depth, μm	34.30	34.50	39.50
	Volumetric wear, 10^{-6} mm^3	3688	3340	3779
	Wear rate, 10^{-6} mm^3/10^3 cycles	1.59	3.15	37.67

scar depth (18%) has to be taken into account. In addition, this standard deviation was obtained for the tests carried out over 150 mm diameter sheaves, so it would be expected a greater standard deviation for tests performed over 100 mm diameter sheaves, where the contact pressure will be greater.

As far as the volumetric wear is concerned, its evolution is similar to this that presented the planimetric wear in line contacts: for tests carried out over 200 and 150 mm diameter sheaves, an initial very short stage where the volumetric wear value increases quickly up to 1.1×10^{-3} mm^3 can be seen, followed by linear (constant slope) behavior. For tests accomplished over the smallest sheaves, the initial short stage is not identified. The volumetric wear exhibits a linear behavior from the beginning. If the tests with different sheaves diameter are compared, a substantial variation in the wear rate can be observed, mainly for tests performed over 100 mm diameter sheaves: if the sheaves diameter is reduced from 200 mm up to 150 mm, the wear rate is multiplied by a factor of two. However, if the sheaves diameter is reduced from 150 mm up to 100 mm, the wear rate is multiplied by a factor of 12 (Table 3). The effect of the sheave diameter is similar to the effect observed for the planimetric wear in linear wear scars and can be clearly seen in Fig. 15, where the volumetric wear of all tests is represented in the same graphic. Due to the large range covered by the number of cycles, the abscise axis had to be represented in logarithm scale. It can be seen how the number of cycles required to obtain the same volumetric wear decreases as the sheaves diameter are reduced, mainly when the sheaves diameters are reduced from 150 to 100 mm.

3.3 Nick Type B

These wear scars present a hyperbolic paraboloid shape, with the ratio of the major axis to minor axis about 2.2. Taken into account the construction of the studied rope, the nick type B should, a priori, be the most dangerous wear pattern, because the crossing angle between the contacting wires is the biggest among all the wear patterns. This fact implies a small contact area, higher contact pressure and, hence, a deeper wear scar. Anyway, the effects of the polymer sheath have to be analyzed.

After having checked the scattering in the different parameters of nicks type A, the selected parameter for the characterization of this wear pattern is the volumetric wear. Alike for nick A, the sensitivity of the topographic measurements was checked measuring a single wear scar three times: the standard deviation for the wear scar depth measurements was below 2%, and below 3% for volumetric wear results.

After having analyzed all the specimens, only a few wear scars of this type were found: the greater part of these wear scars were identified in the specimens obtained from the tests performed over 200 mm diameter sheaves, but only in those that suffered more than 400×10^3 cycles and with important scattering that does not allow deriving any tendency (Fig. 16); in the specimens obtained from the tests performed over 150

mm diameter sheaves, only four dispersed wear scars were found; and in the specimens obtained from the tests performed over 100 mm diameter sheaves and, after several examinations with SEM, no wear scar was detected (Table 4). In addition, the maximum wear scar depth measured is 23 μm, a smaller value than the maximum obtained for nicks type A (40 μm).

Surprisingly, these results establish that the utilization of 200 mm diameter sheaves help the creation of this wear pattern and contradict the results obtained for nicks type A. In addition, these results show that nicks type A are more severe than nicks type B. The reason of this strange behavior is the presence of the polymeric sheath covering the wire rope. A small gap exists between adjacent strands and the polymeric cover can enter into this gap, avoiding the interstrand contact during thousands of cycles (depending on the test conditions) and delaying the nick type B creation. That is why nicks type B appear only in specimens tested during high number of cycles. Also the polymeric sheath is the reason of the high scattering: while the rope segments were being disassembled, how the thickness of the polymeric sheath varied along the perimeter was observed as well as the different penetration of the polymeric sheath into the gaps. Therefore, due to the different penetrations of the polymeric cover into the gaps, the interstrand contact can occur at different number of cycles in the same segment, depending on the perimetrical location.

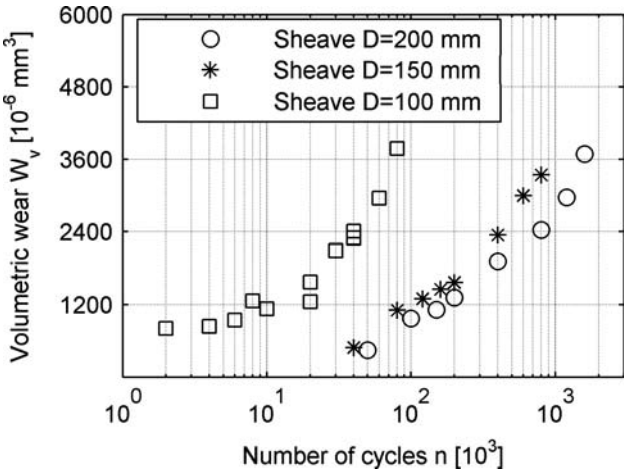

Fig. 15 Nick type A. Volumetric wear in all tests

4. Conclusions

The BoS fatigue tests were successfully accomplished and the evolution of the different wear patterns was studied. The most suitable parameters to characterize the wear behavior are wear scar depth and volumetric wear (planimetric wear for linear wear scars). Planimetric and volumetric wear present an acceptable scattering and a linear evolution. On the other hand, the wear scar depth, although the scattering it is bigger, represents the reduction of the cross section of wires.

Focussing the attention on the wear scar depth, the most dangerous wear pattern for this rope corresponds to nicks type A, in which the wear scar depth achieves a maximum value about 40 μm, while nicks type B achieve a maximum value about 23 μm. In linear wear scars, the maximum value of this parameter is rather smaller (8 μm). From this study, the importance of the polymeric sheath can be derived: although, a priori, nick B should be the most dangerous wear pattern, the polymeric cover enter into the gap between adjacent strands, avoiding the contact during thousands of cycles and delaying the nick B creation.

Finally, the effect of sheave diameter on nicks type A evolution has to be pointed up. If the ratio D/d is reduced a 25% (from 40 to 30), the volumetric wear rate increases approximately 100%, whereas a reduction of 50% the ratio D/d (from 40 to 20) causes an approximate increase of 2200% in the volumetric wear rate.

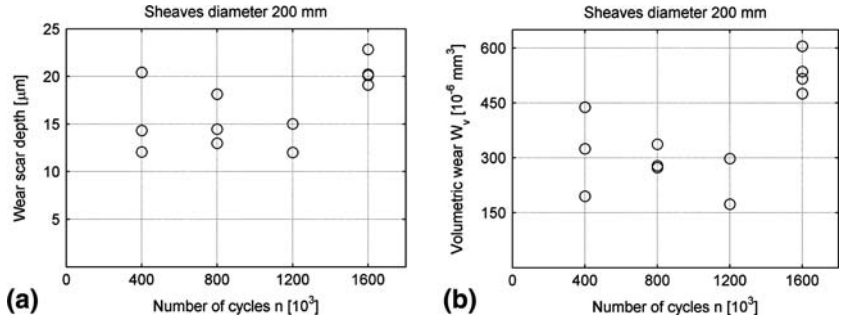

Fig. 16 Nick type B. Wear scar depth and volumetric wear in specimens obtained from tests performed over 200 mm diameter sheaves

Table 4 Nick type B: Results summary

		Sheaves diameter, mm		
		200	**150**	**100**
Nick type B	Maximum number of cycles, 10^3	1600	800	80
	Wear scar depth, μm	22.80	···	···
	Volumetric wear, 10^{-6} mm^3	605	···	···
	Wear rate, 10^{-6} mm^3/10^3 cycles	···	···	···

Future work needs to concentrate on the description of the relationship between the volumetric wear (W_v) and the geometrical parameters (axes dimensions and wear scar depth). If the friction force and sliding amplitude between contacting wires were known in each test, the relationship between volumetric wear and dissipated friction energy could also be checked.

Acknowledgments

This research is sponsored by the Basque Government under the Universidad Empresa programme (Ref. UE2004-6). The authors gratefully acknowledge the support of Orona S. Coop. Also the technical assistance of Mr. J. Salegui (from Mondragon Goi Eskola Politeknikoa) is gratefully acknowledged.

References

1. *Wire Rope Users Manual*, Committee of Wire Rope Producers, American Iron and Steel Institute, Washington, D.C., 1979
2. R.B. Waterhouse, *Fretting Corrosion*. Pergamon Press, Oxford, 1972
3. R.B. Waterhouse, *Fretting Fatigue*. Applied Science Publishers LTD, London, 1981
4. B.R. Pearson, P.A. Brook, and R.B. Waterhouse, Fretting in Aqueous Media Particularly of Roping Steels in Seawater, *Wear*, 1985, **106**(1–3), p 225–260
5. R. Smallwood and R.B. Waterhouse, Residual Stress Patterns in Cold Drawn Steel Wires and Their Effect on Fretting-Corrosion-Fatigue Behaviour in Seawater, in *Applied Stress Analysis*, T.H. Hyde and E. Ollerton, Eds., Elsevier Applied Science, 1990, p 82–90
6. S.J. Harris, R.B. Waterhouse, and I.R. McColl, Fretting Damage in Locked Oil Steel Ropes, *Wear*, 1993, **170**(1), p 63–70
7. R.E. Hobbs and M. Raoof, Mechanism of Fretting Fatigue in Steel Cables, *Int. J. Fatigue*, 1994, **16**(4), p 273–280
8. R.B. Waterhouse, Fretting in Steel Ropes and Cable—A Review, *ASTM Spec. Tech. Publ.*, 2002, **1425**, p 3–14
9. C.R. Chaplin and A. Potts, Wire Rope Offshore—A Critical Review of Wire Rope Endurance Research Affecting Offshore Applications, UK Health & Safety Executive (HSE), Offshore Technology Report OTH 91 341, 1991
10. I.M.L. Ridge, J. Zheng, and C.R. Chaplin, Measurement of Cyclic Bending Strains in Steel Wire Rope, *J. Strain Anal. Eng. Des.*, 2000, **35**(6), p 545–558
11. I.M.L. Ridge, C.R. Chaplin, and J. Zheng, Effect of Degradation and Impaired Quality on Wire Rope Bending over Sheave Fatigue Endurance, *Eng. Fail. Anal.*, 2001, **8**(2), p 173–187
12. K. Feyrer, Statistical Evaluation of the Results of Wire Rope Bending Tests—1, *Wire*, 1981, **31**(3), p 118–121
13. K. Feyrer, Statistical Evaluation of the Results of Wire Rope Bending Tests—2, *Wire*, 1981, **31**(4), p 158–162
14. K. Feyrer, Calculation of Rope Drives, *Wire*, 1983, **33**(2), p 35–37
15. K. Feyrer, The Number of Bending Cycles to Breakage of Parallel Lay Wire Ropes, *Wire*, 1985, **35**(5), p 198–202
16. K. Feyrer, Endurance Calculation of Wire Ropes Running over Sheaves, *Wire*, 1995, **45**(2), p 99–103
17. K.K. Schrems, Wear Related Fatigue in a Wire Rope Failure, *J. Test. Eval.*, 1994, **22**(5), p 490–499
18. K.K. Schrems and D. Maclaren, Failure Analysis of a Mine Hoist Rope, *Eng. Fail. Anal.*, 1997, **4**(1), p 25–38
19. M. Torkar and B. Arzensek, Failure of Crane Wire Rope, *Eng. Fail. Anal.*, 2002, **9**(2), p 227–233
20. P. Parameswaran, V.S. Raghunathan, S.C. Hiremath, and K.R. Paknikar, Failure of Locked Coil Wire Rope of Coal Handling System, *Eng. Fail. Anal.*, 2003, **10**(4), p 395–404
21. K.K. Schrems, C.P. Dogan, and J.A. Hawk, Wear Mechanisms in a Nonrotating Wire Rope, *J. Mater. Eng. Perform.*, 1995, **4**(2), p 136–144
22. "Safety rules for the construction and installation of lifts—Part 1: Electric lifts," UNE EN 81–1 2001, p 12–176
23. Sensofar Corporation Website. http://www.sensofar.com/ [accessed 11 April 2007]
24. M.A. Urchegui, W. Tato, and X. Gómez, A Method for Evaluating Fretting Wear Scars in Thin Steel Roping Wires Based On Confocal Imaging Profilometry, *J. Test. Eval.*, 2007, **35**(4), p 357–363
25. T. Liskiewicz and S. Fouvry, Development of a Friction Energy Capacity Approach to Predict the Surface Coating Endurance Under Complex Oscillating Sliding Conditions, *Tribol. Int.*, 2005, **38**(1), p 69–79
26. C. Paulin, S. Fouvry, and S. Deyber, Wear Kinetics of Ti-6Al-4V Under Constant and Variable Fretting Sliding Conditions, *Wear*, 2005, **259**(1–6), p 292–299
27. A. Ramalho and J.C. Miranda, The Relationship Between Wear and Dissipated Energy in Sliding Systems, *Wear*, 2006, **260**(4–5), p 361–367